Soft Matter

The nonequilibrium behaviors of covalent adaptable network polymers during the topology transition

Journal:	*Soft Matter*
Manuscript ID	SM-ART-08-2020-001471.R2
Article Type:	Paper
Date Submitted by the Author:	17-Dec-2020
Complete List of Authors:	Shi, Xiaojuan; University of Colorado at Denver - Anschutz Medical Campus, Mechanical Engineering Ge, Qi; Southern University of Science and Technology, Department of Mechanical and Energy Engineering Lu, Haibao; Harbin Institute of Technology, National Key Laboratory of Science and Technology on Advanced Composites in Special Environments Yu, Kai; University of Colorado at Denver - Anschutz Medical Campus, Mechanical Engineering

SCHOLARONE™
Manuscripts

The nonequilibrium behaviors of covalent adaptable network polymers during the topology transition

Xiaojuan Shi[1,2], Qi Ge[3], Haibao Lu[2,*], Kai Yu[1,*]

1. Department of Mechanical Engineering, University of Colorado Denver, Denver, CO 80217, USA

2. National Key Laboratory of Science and Technology on Advanced Composites in Special Environments, Harbin Institute of Technology, Harbin, 150080, PR China

3. Department of Mechanical and Energy Engineering, Southern University of Science and Technology, Shenzhen, Guangdong, China

* *Corresponding author HBL: luhb@hit.edu.cn; KY: kai.2.yu@ucdenver.edu*

Abstract: Vitrimer with bond exchange reactions (BERs) is a type of covalent adaptable network (CANs) polymers at the forefront of recent polymer research. They exhibit malleable and self-healable behaviors and combine the advantages of easy processability of thermoplastics and excellent mechanical properties of thermosets. For thermally-sensitive vitrimers, a molecular topology melting/frozen transition is triggered when the BERs are activated to rearrange the network architecture. Notable volume expansion and stress relaxation are accompanied, which can be used to identify the BER activation temperature and rate, as well as to determine the malleability and interfacial welding kinetics of vitrimers. Existing works on vitrimers reveal the rate-dependent behaviors of the nonequilibrium network during the topology transition. However, it remains unclear what the quantitative relationship with heating rate is, and how it will affect the macroscopic stress relaxation. In this paper, we study the responses of an epoxy-based vitrimer subjected to a change in temperature and mechanical loading during the topology

transition. Using thermal expansion tests, the thermal strain evolution is shown to depend on the temperature-changing rate, which reveals the nonequilibrium states with rate-dependent structural relaxation. The influences of structural relaxation on the stress relaxation behaviors are examined in both uniaxial tension and compression modes. Assisted by a theoretical model, the study reveals how to tune the material and thermal-temporal conditions to promote the contribution of BERs during the reprocessing of vitrimers.

Keywords: *Structural relaxation, topology transition, stress relaxation, BER activation temperature, covalent adaptable network polymers*.

1. Introduction

Polymers with covalently crosslinked networks are conventionally defined as thermosets [1, 2]. They are ideal for engineering applications that require high mechanical strength, thermal stability, and chemical resistance. However, the networks are permanently "set" after polymerization and thus cannot be melted and reprocessed as thermoplastics [3]. Very recently, this picture has been changed by incorporating reversible covalent bonds into polymer networks [4-20]. Such covalent adaptable networks (CANs) [7, 18, 21] are crosslinked thermosets, but possess the dynamic reversible bonds that allow the continuous rearrangement of network topology. A prominent example is the recently developed vitrimer networks with associative cross-links. The network rearrangement is enabled through bond exchange reactions (BERs) with a simple stimulus (*e.g.,* temperature) while the overall network connectivity and crosslinking density are maintained. When such macromolecular events occur in large amounts, they can attribute to unusual properties that are not seen in conventional thermosetting polymers, such as malleability [6, 7, 16, 18, 22-27], interfacial welding [28-43], and network decomposition in a specific solvent [43-47].

The innovative properties of CANs have enabled their emerging applications. For example, the interfacial welding and network decomposition were utilized to reprocess, repair, and recycle thermoset wastes [20, 48-56]. The stress relaxation and malleability features were applied to design shape-changing materials and structures [6, 7, 16, 18, 22-27, 57-60]. Recently, CAN hydrogels have been used as the extracellular matrix for biomedical applications due to their tunable mechanical properties and adaptability to neighboring tissues [61-66]. When the dynamic networks of vitrimers are utilized to design

their myriad applications, the BER activation temperature and BER rate are the primary quantities to characterize, which serve as a foundation to understand the rate of network rearrangement, self-healing, and recycling performance with different material and processing parameters [67-77].

Simple and standard mechanical tests have been employed to characterize vitrimers. For example, the BER activation temperature, which is normally above the network glass transition temperature, can be readily probed using thermal expansion tests [18, 19, 21]. For conventional thermosets in the rubbery state, the free volume of polymer chains increases with temperature due to their enhanced vibrational motion. At a moderate temperature-changing rate, a linear relationship can be observed between the thermal strain and temperature. However, for vitrimers, a molecular topology melting/frozen transition is triggered when the BERs are activated to rearrange the network architecture [18, 19, 21, 78]. As pointed out by Montarnal et al. [18], while a vitrimer maintains the network overall crosslinking density at high temperatures, the network topology is dynamic, and the active BERs enable the crosslinked network to behave like an un-crosslinked thermoplastic. During a dilatometry experiment, cross-linked networks are known to exhibit a lower expansion coefficient than the corresponding non–crosslinked polymers because the crosslinking sites restrict the vibration of monomers and polymer chains. In terms of this, the BERs lead to an additional increment in the free volume of polymer chains for their vibrational motion by reducing the restrictions, and thus the macroscopic volume of vitrimers is increased. The BER activation temperature can be defined at the temperature when the slope of the thermal strain curve starts to increase dramatically. To characterize the rate of BERs, a common practice is to employ the stress relaxation tests at different

temperatures [52, 67, 79, 80]. The stress dropping rate is proportional to the rate of BERs within the network. A BER activation energy can be determined by measuring the relaxation times at different temperatures.

The dynamics of vitrimer networks is shown to depend on various influencing parameters. First, the rate of BER can be promoted by temperature [18]. Increasing the catalyst content or using efficient organic catalysts will reduce the energy barrier for BERs and decrease the BER activation temperature [19, 21] Second, previous studies also showed that the dynamics of vitrimer depends on the thermal history. For example, Montarnal et al. [18] performed dilatometry tests on the vitrimer and showed that when the heating rate was increased from 0.2K/min to 1K/min, the BER activation temperature was increased by ~ 17^{o}C. Kaiser et al. [81] observed a similar phenomenon, wherein the BER activation temperature was measured by creep tests. Fang et al. [82] examined the influence of vitrimer topology on its rheological properties using small-amplitude oscillatory shear tests. At BER activation temperature, they found that the material was in a critical state, and the dynamic modulus was independent of the testing frequency. The vitrimer was shown to exhibit different activation temperatures in the cooling cycle and heating cycle. All these pioneering studies reveal the rate-dependency of vitrimer and suggest that the network structure is in the nonequilibrium state during the topology transition. However, fundamental questions remain unclear. For example, what is the quantitative relationship between the BER activation temperature, temperature changing rate, and catalyst content? Does the activation temperature keep increasing with the heating rate? How will the non-equilibrium thermal expansion affect the macroscopic stress relaxation of vitrimers? During the stress relaxation in tension, both structural relaxation and BERs release the

internal stress with confined boundary conditions, but it is only the BER that contributes to the network malleability and reprocessing, while the structural relaxation is temporary and reversible when the temperature returns to the room temperature. On the other hand, if the compressive stress is used, CANs could already be effectively processed even without dramatic stress releasing. Answers to these questions play a critical role in understanding material properties and guide the applications of vitrimers in thermally reforming and reprocessing thermosetting polymers.

In this paper, we present a detailed study of the nonequilibrium behaviors of vitrimers during their topology transition. Using thermal expansion tests, we show that the thermal strain evolution highly depends on the temperature-changing rate, which suggests nonequilibrium networks with rate-dependent structural relaxation. Therefore, the probed BER activation temperature depends not only on the catalyst content but also on the thermal history. The influences of time-dependent structural relaxation on the network stress relaxation behaviors are examined in both uniaxial tension and compression modes. A theoretical model based on the concept of fictive temperature is defined to assist the analysis and discussion. We show that the simple modeling framework can be used to precisely capture the experimental results on both thermal expansion and stress relaxation. It is further applied to unravel the coupled effect of structural relaxation and BERs on the stress relaxation behavior of vitrimers.

2. Materials and Experiments

2.1 Material synthesis

The material used in this study is an epoxy-based vitrimer developed by Leibler and

coworkers [16]. The epoxy samples were synthesized with the monomer diglycidyl ether of bisphenol A (DGEBA, Sigma Aldrich, St. Louis, MO), the crosslinker fatty acids (Pripol 1040, Croda, Houston, TX), and the catalyst for transesterification BERs ($Zn(Ac)_2$, Sigma Aldrich).

Three groups of epoxy samples were prepared with different catalyst contents. The mole ratios between DGEBA and catalyst were 1%, 5%, and 10%, respectively. A higher catalyst content enables faster BERs within the network at an equivalent temperature. For polymer synthesis, all the epoxy samples with different catalyst stoichiometry were prepared following the same procedure. The catalyst was first mixed with the fatty acid in a beaker. The temperature was gradually increased from 100°C to 150°C while maintaining the mixture under vacuum until no gas evolution was observed and the catalyst particles were completely dissolved (3 hours). DGEBA was then added to the fatty acid mixture containing solubilized catalyst (stoichiometry between COOH and DGEBA is 1:1) in a round-bottom flask and manually stirred until the mixture became homogeneous. Finally, the mixture was poured into a mold and placed in an oven for 6 h at 130°C.

A control epoxy sample was synthesized without the BER catalyst. The ratio between the fatty acid and DGEBA was the same as that in the epoxy vitrimer samples. Without the catalyst, no BER would be triggered at high temperature, and the material behaves like conventional thermosetting polymers.

2.2 Thermal expansion measurements

The volume change of vitrimer samples during the structural relaxation was characterized using the thermal expansion tests. The samples were heated at the free-

standing state using a Dynamic Mechanical Analysis (DMA, Model Q800, TA Instruments, New Castle, DE, USA) tester. The sample length change was recorded and used to calculate the coefficient of thermal expansion. Note that the coefficient of thermal expansion is commonly determined by measuring the change of sample specific volume, which is approximately three times of the change in sample length within the scope of small deformation. However, as will be shown in the following sections, this study focuses on 1D mechanical problems (e.g., stress relaxation in tension and compression). Therefore, the 1D linear thermal expansion coefficient is used to characterize the degree of sample thermal expansion. When it comes to the 3D mechanical problems, the coefficient of thermal expansion should be obtained by measuring the specific volume.

Two types of temperature profiles were used during the thermal expansion measurements. In the first one, the vitrimer samples were subject to heating/cooling cycles with the temperature changed between 140°C and 220°C in a stepped manner. The temperature interval was 20°C. When the target temperature was reached, a 40 min isothermal stabilization time was given before proceeding to the next temperature at 10°C /min. In the second one, the temperature was continuously increased from 80°C to 250°C with a heating rate of 0.5, 1, 2, 5°C /min, respectively.

2.3 Stress relaxation tests in tension

The stress relaxation tests were conducted using the DMA tester in the tension state. The vitrimer samples were cut into the same dimension (10 mm in length, 3 mm in width, and 0.8 mm in thickness). During the tests, the strain amplitude was set to be 5%, and the stress relaxation time was set to be 90 min for all cases. The drop in stress was recorded to

calculate the relaxation modulus.

Two types of temperature profiles were used during the measurements. In the first one, vitrimer sample with 10 % mole catalyst was first heated from room temperature to 180°C at 20°C/min, and then stabilized at the same temperature for different times (0 min, 3 min, 6 min, 8 min, 11 min, 15 min, and 20 min, respectively) prior to the stress relaxation tests. In the second group of tests, the epoxy samples with different catalyst contents were first heated from room temperature to the testing temperature (140°C, 160°C, 180°C, 200°C, and 220°C, respectively) at 20°C/min, and then followed by an isothermal stabilization step for 5 min. After that, the strain was applied, and the stress variation was monitored and recorded.

2.4 Stress relaxation tests in compression

Stress relaxation tests in compression were performed using an Electro-Force machine (Bose Electro Force 3200, Eden Prairie, MN, USA) equipped with an Instron SFL Temperature Controlled Chamber (Model 3119-405-21). All the vitrimer samples were cut into the same cubic geometry (5 mm in length, 5 mm in width, and 5 mm in height). Prior to the test, the sample was first heated from room temperature to the testing temperature (140°C, 160°C, 180°C, 200°C, and 220°C, respectively) at 20°C/min. After stabilizing at the testing temperature for 5 min, a 5% compressive strain was then applied and maintained for 90 min, with the stress being monitored and recorded.

3. A theoretical model for structural relaxation and stress relaxation

3.1 Modeling the structural relaxation based on experimental observations

Before we define the theoretical model for structural relaxation, the strain evolutions of epoxy samples during the thermal expansion measurements are shown in Fig 1a. The experimental data of the control sample without catalyst and the vitrimer sample with 10% catalyst is presented. The temperature was continuously increased from 80 °C to 250 °C. The heating rate was 0.5°C /min (solid lines) and 5°C /min (dashed lines), respectively. Note that the vitrimer samples with different catalyst contents exhibit a close T_g around 30°C (see the supplementary material, Section S1), which suggests that at the starting temperature 80°C, all the samples exhibit near-identical rheological properties and thermal expansion behaviors.

There are two interesting characteristics that can be revealed from the figure. First, for the control sample without the catalyst, the thermal strain is observed to increase linearly with the temperature, which is consistent with the response of conventional thermosets at the rubbery state. However, the thermal strain of the vitrimer sample shows a non-linear response to the temperature. The strain first increases with a constant rate and then increases dramatically when the BER is activated during the topology transition. Second, the thermal strain evolution of the vitrimer sample highly depends on the heating rate, namely a time-dependent response to the temperature change. With a higher heating rate, the increment of thermal strain is delayed. For the control sample, even though the temperature is high above its glass transition temperature (T_g, ~20°C), there is still a notable difference between the two curves with different heating rates.

The thermal strain evolution of the vitrimer sample is subtracted by that of the control sample with the same heating rate and plotted in Fig. 1b. Since the control sample has the network structure as the vitrimer sample but without BER, Fig. 1b essentially represents

the additional thermal strain produced by the BER and network rearrangement during the topology transition. As shown in the figure, this portion of thermal strain increases with temperature exponentially and decreases with the heating rate.

Based on the experimental observations, we define the theoretical model for structural relaxation, wherein the thermal strain (ε_T) is split into two parts:

$$\varepsilon_T(T,t) = \varepsilon_{TT}(T,t) + \varepsilon_{BT}(T,t). \quad (1)$$

In the above equation, ε_{TT} is the intrinsic thermal strain produced by the vibrational motion of polymer chains, which essentially represents the thermal response of the control sample. ε_{BT} is the additional thermal strain resulting from the BERs and topology rearrangement. Both parts depend on temperature and time. Note that for conventional thermosets without BERs, their thermal strain only changes with temperature. But for the control epoxy networks used in this study, a slight difference in the thermal strain evolution is observed at different heating rates (Fig. 1a). Therefore, ε_{BT} is also assumed to be a rate-dependent parameter.

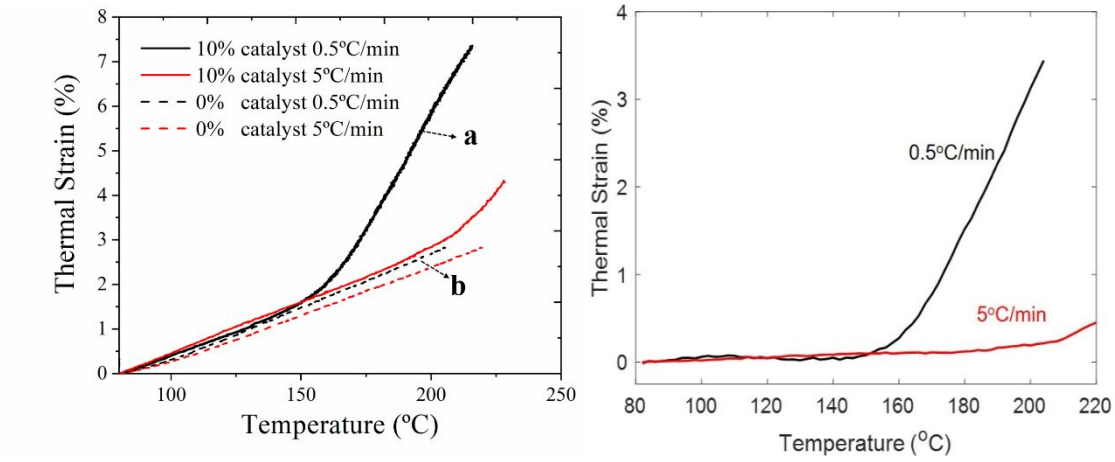

(a) (b)

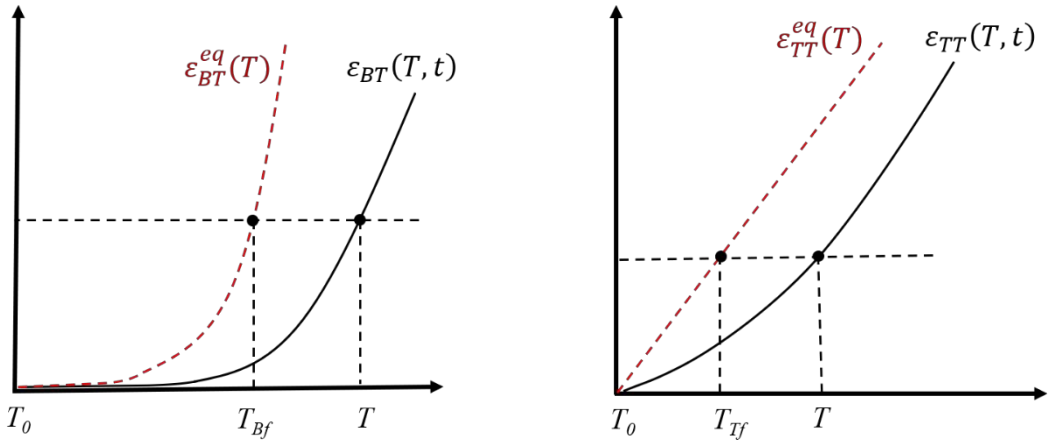

Fig. 1. (a) *The experimental data of strain evolutions of control sample without catalyst and the vitrimer sample with 10% catalyst.* ***(b)*** *The difference in the thermal strain evolution between control sample and the vitrimer sample with 10% catalyst. The curve was obtained by subtracting the thermal strain curve of vitrimer sample by that of the control sample with the same heating rate. Illustrations of the concept of fictive temperature for* ***(c)*** *BER-induced structural relaxation and* ***(d)*** *intrinsic structural relaxation of control sample.* ε_{BT}^{eq} *and* ε_{TT}^{eq} *represent the thermal responses in the equilibrium state, namely when the heating rate is infinitely small.*

To describe the evolution of ε_{TT} and ε_{BT} with different heating rates, we adopt the concept of fictive temperature, which was first introduced by Tool et al. [83] to study the nonequilibrium structure of glasses. The fictive temperature represents the temperature at which the nonequilibrium structure at T is in equilibrium. When it is applied to the viscoelasticity of polymers, it has been proven that different thermomechanical properties (such as volume, density, and modulus) of a given polymer may have different fictive temperatures [84, 85]. For the structural relaxation of vitrimers, since it involves two types of thermal strains with distinguished physical mechanisms, we propose to use two fictive

temperatures, T_{Bf} and T_{Tf}, to respectively describe the evolution of ε_{TT} and ε_{BT}. The fictive temperature T_{Tf} is corresponding to the intrinsic thermal expansion of polymer networks resulted from chain vibration, and T_{Bf} is corresponding to the BERs that releasing the restrictions on the thermal vibration of polymer chains. Their significances are shown in Figs. 1c and 1d. In both two figures, ε_{BT}^{eq} and ε_{TT}^{eq} are the thermal strain evolution in the equilibrium state, namely when the temperature-changing rate is infinitely low.

The relaxation of the nonequilibrium network to its equilibrium configuration is modeled as the time evolution of fictive temperatures to T. Following the previous work by Tool [83], the following evolution equations are used for T_{Bf} and T_{Tf}:

$$\frac{dT_{Tf}}{dt} = \frac{1}{\tau_{TR}}\left(T - T_{Tf}\right), \tag{2b}$$

$$\frac{dT_{Bf}}{dt} = \frac{1}{\tau_{BR}}\left(T - T_{Bf}\right). \tag{2b}$$

For the vitrimer CAN initially at T_0, we have $T_{Bf} = T_{Tf} = T_0$. The parameter τ_{TR} and τ_{BR}, commonly referred to as the structural relaxation times, are the characteristic retardation time of the volume changes due to intrinsic thermal expansion and BER-induced topology transition, respectively. We assume both relaxation times following the time-temperature superposition principle (TTSP), namely

$$\tau_{TR} = \tau_{TR\_0}\alpha_T(T), \tag{3a}$$

$$\tau_{BR} = \tau_{BR\_0}\alpha_B(T) \tag{3b}$$

where τ_{TR_0} and τ_{BR_0} are reference relaxation time, which are different for the intrinsic network thermal expansion and BER-induced structural relaxation. α_T and α_B a are the shift factors. The structural relaxation time τ_{TR} is a macroscopic measure of the molecular

mobility, so the Williams-Landel-Ferry (WLF) equation can be used to describe its temperature dependency. On the other hand, since the relaxation time τ_{BR} is related to the kinetics of covalent exchangeable reactions, an Arrhenius' law is adopted for the α_B:

$$\log \alpha_T(T) = \frac{-C_1\left(T - T_0\right)}{C_2 + \left(T - T_0\right)}, \tag{4a}$$

$$\ln \alpha_B(T) = \frac{E_a}{R}\left(\frac{1}{T} - \frac{1}{T_0}\right). \tag{4b}$$

Here, E_a is the BER activation energy. C_1 and C_2 are fitting parameters. R is gas constant (8.314 $J{\cdot}K^{-1}{\cdot}mol^{-1}$).

Based on the observations of strain evolutions in Fig. 1a and 1b, a linear equation is used to formulate the strain evolution of the control sample in the equilibrium state, and an exponential function is used for the BER-induced strain evolution.

$$\varepsilon_{BT}\left(T,t\right) = \beta\left\{\exp\left[\alpha\left(T_{Bf} - T_0\right)\right] - 1\right\}, \tag{5a}$$

$$\varepsilon_{TT}\left(T,t\right) = -\alpha_n\left(T_{Tf} - T_0\right), \tag{5b}$$

where α and β are the fitting parameters. α_n is the coefficient of thermal expansion of control sample in the rubbery state, which can be measured from the thermal expansion tests. Overall, the fictive temperatures serve as an internal variable describing the evolution of the nonequilibrium structure.

3.2 Stress relaxation coupled with structural relaxation

To study the mechanical response of vitrimers coupled with structural relaxation, the following 1D thermoviscoelastic rheological model is used (Fig. 2). A thermal expansion element is arranged in series with mechanical elements. The thermal expansion element

describes the thermal strain during the structural relaxation, which is defined in Section 3.1. The mechanical elements describe the BER-induced stress relaxation of vitrimers. Within the dynamic networks, the relaxation time depends on the chain mobility, which is a function of chain length. Since the chain length within a real polymer network is not uniform, multiple thermo-viscoelastic nonequilibrium branches are adopted in the mechanical component. Different branches are arranged in parallel within the model, and each branch has a distinguished modulus (E_i) and relaxation time (τ_i).

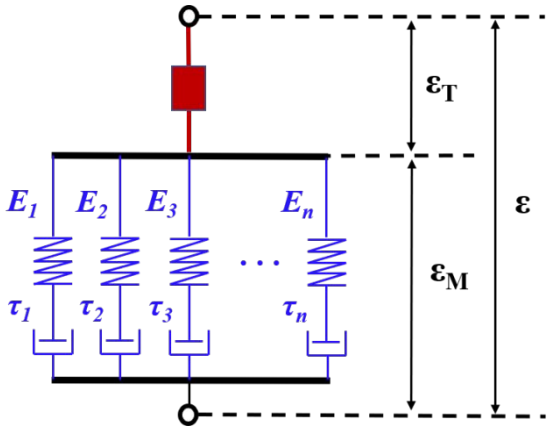

Fig. 2 *The thermoviscoelastic rheological model to study the mechanical response of CANs coupled with structural relaxation.*

In this paper, the strain amplitude during the stress relaxation tests is 5%. Therefore, a linear viscoelasticity stress-strain relationship is defined for the modeling framework. A nonlinear stress-strain relationship could also be defined for the case of large deformation, as shown in the previous works.

The total stress σ of the multi-branch model is the summation of each branch, σ_i:

$$\sigma = \sum_{i=1}^{n} \sigma_i = \sum_{i=1}^{n} E_i \varepsilon_{Mi} \,, \tag{6}$$

where the ε_{Mi} is the mechanical strain of the *i*-th branch, namely the strain of the elastic spring.

The stress-strain evolution in *i*-th branch follows the governing equation:

$$\frac{d\sigma_i}{dt} = E_i \frac{d\varepsilon_{Mi}}{dt} - \frac{\sigma_i}{\tau_i}. \tag{7}$$

The stress relaxation time, τ_i, follows the Arrhenius-type TTSP:

$$\tau_i(T) = \tau_{i0}\alpha_B(T), \tag{8}$$

where τ_{i0} is a reference relaxation time at T_0. $\alpha_B(T)$ is the same shift factor for BERs defined in Eq. 4b.

There are two groups of parameters in the theoretical model. As shown in the following sections, parameters for the structural relaxation can be determined from the experimental results of thermal expansion. Parameters for the BER-induced stress relaxation can be determined by the stress-relaxation tests. All parameters are listed in the Appendix, Table 1.

4. Results and Discussion

4.1 Thermal strain responses during the structural relaxation

4.1.1 Thermal strain evolution during the stepped heating

Figs. 3a, 3c, 3e, and 3g show the strain evolution of vitrimer samples and control sample during a heating-cooling cycle with stepped temperature-changing profile. The temperature changed between 140 °C and 220 °C and the temperature interval was 20 °C. When a target temperature was reached, a 40 min isothermal stabilization time was given before proceeded to the next temperature at 10 °C /min.

During the heating process, it is observed that the thermal strain of all samples increases with temperature. The strain keeps increasing during the isothermal stabilization, which suggests nonequilibrium networks with structural relaxation. The net strain increments in each isothermal step (i.e., the differential thermal strain) are plotted in Figs. 3b, 3d, 3f, and 3h as a function of stabilization time. For the vitrimer samples, the speed of structural relaxation increases with the temperature and catalyst content. This can be told by comparing the slopes of the thermal strain curves in Fig. 3b, 3d, and 3f. During the stepped heating process, the vitrimer cannot fully equilibrate before moving to the next heating step. Therefore, at a relatively higher temperature, the vitrimer is further away from its equilibrium state and thus requires more time to fully equilibrate. For the control sample, it is interesting to observe that the strain increments at all isothermal temperatures are nearly identical, reaching a saturated value of ~0.2% after ~10 min stabilization. This suggests that even though there is no BER involved and the material is in the rubbery state, the network still deviates from its equilibrium state due to the fast heating (10 °C /min) prior to the isothermal step.

The thermal strain decreases during the cooling step of vitrimer samples. Since the structural relaxation during the topology transition is time-dependent, there is a hysteresis for the strain evolution. By the end of the cooling step, a residual strain is observed in the vitrimer samples with higher catalyst content. For example, the residual strain in epoxy samples with 10% and 5% catalyst is 1.6% and 0.7%, respectively, while the residual strain in the epoxy sample with 1% catalyst and the control sample is negligible. The residual strain and hysteresis of the vitrimer sample are observed to increase with the catalyst content. This is because the network did not fully reach the equilibrium state before cooling,

so the BER-induced structural relaxation during the cooling step still tends to increase the sample volume. Only the intrinsic thermal strain decreases due to its lower relaxation time. The residual strain and hysteresis of the vitrimer sample are expected to decrease by either decreasing the cooling rate or extending the isothermal stabilization time. In the supplementary material (Section S2, Fig. S2), we performed a thermal expansion test with an extremely low heating rate. During the tests, the vitrimer sample with 10% catalyst was first equilibrated at 160^{o}C for one hour, a period that is long enough to reach the equilibrium state. Then the temperature was increased to 180^{o}C at 0.1^{o}C/min, followed by cooling at the same rate to 160^{o}C. As shown in Fig. S1, the hysteresis between the heating and cooling curves is negligible.

The experimental data can be used to determine the material parameters in the thermal expansion element in Section 3.1. First, by fitting with the thermal strain evolution of the control sample with a low heating rate, 0.5^{o}C/min, the coefficient of thermal expansion, α_n (in Eq. 5b), is determined to be 0.00023 $^{o}C^{-1}$ (see Supplementary Material, Section S3, Fig. S3a). The fitting parameters in the WLF equation, C_1 and C_2 (in Eq. 4a), are determined to be 0.07 and 18^{o}C, respectively. The structural relaxation time, τ_0 (in Eq. 3a), is 0.15s. With these parameters, the model is able to capture the difference in thermal strain evolution between 0.5^{o}C/min and 5^{o}C/min (see Supplementary Material, Section S3, Fig. S3b). Fig. S2c presents the evolution of structural relaxation τ_{TR}. It is observed that the changes are small (~0.15s-~0.1s) within the temperature range 80 ^{o}C -220^{o}C. Note that this relaxation time, τ_{TR}, is not exactly consistent with the relaxation times of epoxy that are reported before. For example, it was shown that when the temperature was high above the network T_g, the relaxation time of epoxy is ~10^{-3} – ~10^{-2}s [86, 87]. The reason is due to the different

physical meaning and characterization methods. In this work, τ_{TR} is corresponding to the time scale of thermal expansion, which results from the thermal vibration of polymer strands. While in previous studies, the relaxation time is corresponding to the stress relaxation, which results from the change of the chain configuration to release the internal stress. There might be some correlation between these two physical mechanisms and relaxation time scales but is beyond the scope of this study and deserves our future study.

By fitting with the strain evolution of vitrimer samples, α and β are determined to be $0.027\ ^{o}C^{-1}$ and $\beta = 0.51$, respectively (in Eq. 5a), and $\tau_{BR_0} = 4.7\times10^{4}$s. Note that the BER activation energy, E_a (in Eq. 4b), depends on the catalyst content. The E_a value for the vitrimer samples with 10%, 5%, and 1% catalyst are 44 *kJ/mol*, 47 *kJ/mol*, and 55 *kJ/mol*, respectively. Note that the determined BER activation energy is much lower compared to the value (~ 80 kJ/mol) reported by Montarnal et al. [18] and Capelot et al. [19, 21] This could result from the different characterization methods employed. In this study, the activation energy is determined by the thermal expansion data, while the previous works typically employed stress relaxation tests. In the Supplementary Material, Fig. S3c also presents the evolution of τ_{BR} of epoxy vitrimer with 10% catalyst. It is observed to decrease with temperature and be 2-3 orders of magnitude higher than τ_{TR}. Because of this, the fictive temperature for BER-induced structural relaxation, T_{Bf}, shows a higher rate-dependency compared to that for intrinsic network thermal expansion, T_{Tf} (Supplementary Material, Section S3, Fig. S3d).

With the determined parameters, the model shows a close prediction on the strain evolutions in Fig. 3. In addition, thermal expansion tests were performed on vitrimer samples with extended isothermal stabilization time. The samples contain 10% and 5%

catalyst, respectively. During the tests, the sample was first stabilized at 180°C for 1 hour, then the temperature was increased to 200°C at 10°C/min. After isothermal stabilization for 120 mins, the temperature was further increased to 220°C at 10°C/min followed by 120 min stabilization. As shown in the Supplementary Material (Fig. S4), the model can closely capture the strain evolution and plateau behavior at 220 and 200 °C.

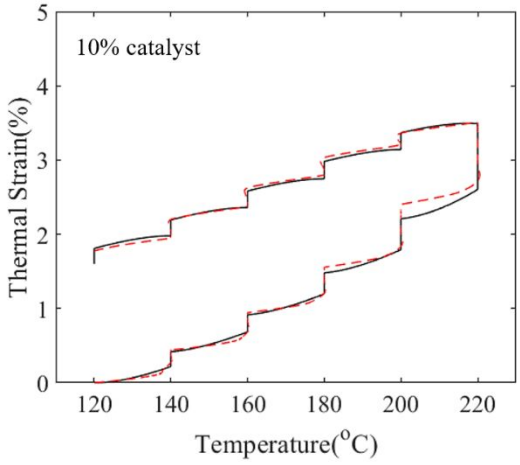

(a)

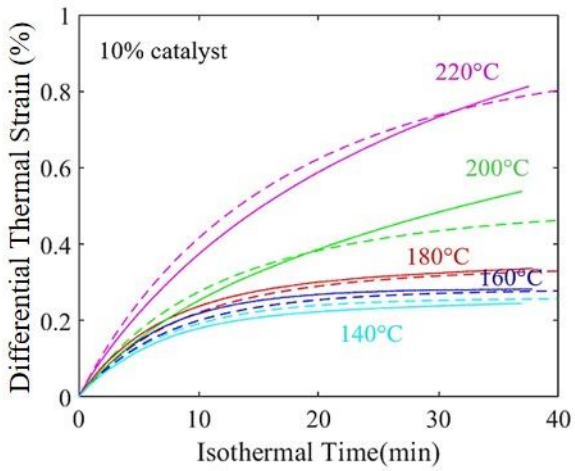

(b)

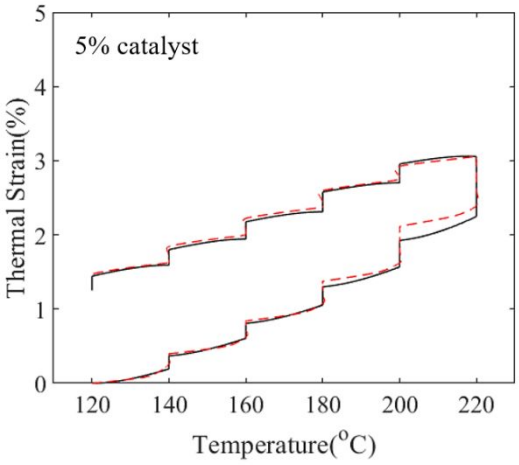

(c)

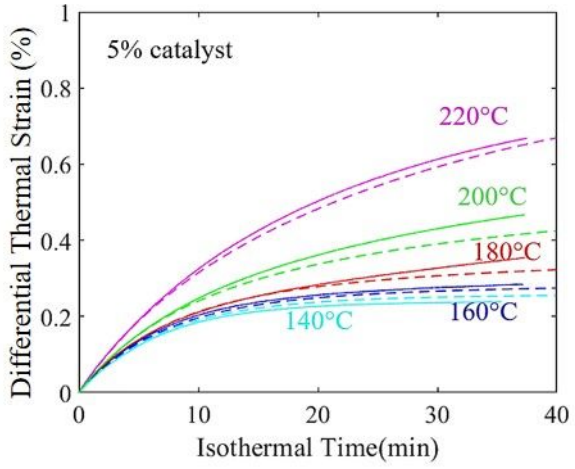

(d)

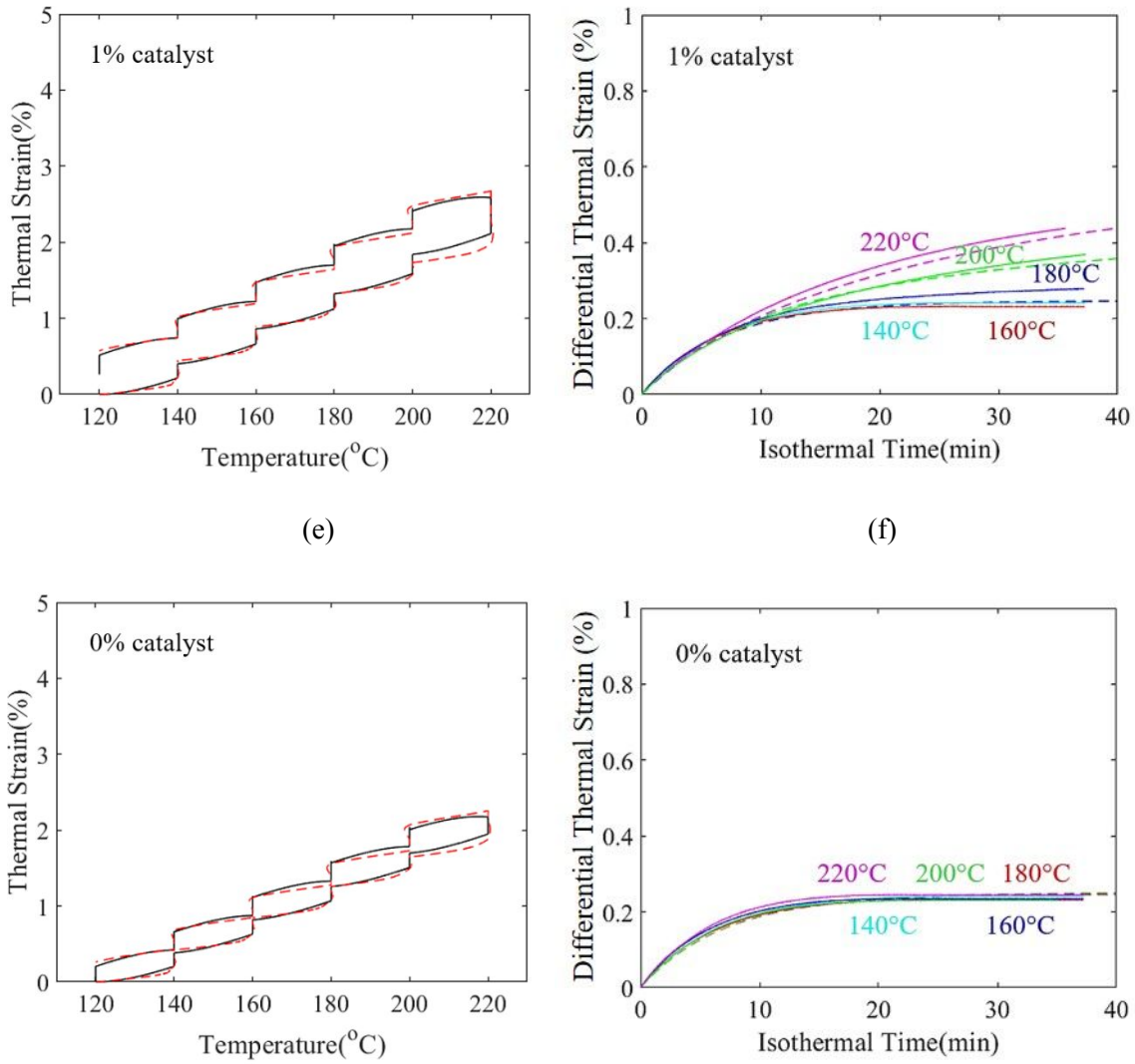

Fig. 3 *Evolution of thermal strain with stepped heating profile. The epoxy samples have different catalyst content (10, 5, 1, and 0 %, respectively). (a), (c), (e), and (g) Thermal strain as a function of temperature. (b), (d), (f), and (h) Thermal strain as a function of isothermal time. Solid lines: experimental results. Dashed lines: predictions.*

4.1.2 Thermal strain evolution during the continuous heating

The thermal strain evolution of vitrimer samples with the continuous heating condition is shown in Fig. 4. Four heating rates were applied for each sample. It is observed that at

the early stage of heating, thermal strain increases almost linearly with temperature. When the temperature is sufficiently high, BERs are activated, and the thermal strain starts to increase dramatically. The increment is higher with more BER catalyst present in the network. For the epoxy vitrimer sample with 1% catalyst, the effect of BER is ineligible, and strain evolution is close to that of the control sample.

In the thermal strain curves, the temperature corresponding to the slope change has been defined as the BER activation temperature (T_{vi}). As the experimental results suggest, the vitrimer sample with a higher catalyst content exhibits a lower T_{vi}. For example, with the same heating rate of 0.5°C/min, T_{vi} decreases from ~170 °C to ~150 °C, when the catalyst content is increased from 5% to 10%. On the other hand, the T_{vi} measured from the thermal expansion tests strongly depends on the heating rate. For the epoxy vitrimer sample with 10% catalyst, the T_{vi} increases from ~150 °C to ~220 °C when the heating rate is increased from 0.5°C/min to 5°C/min. With a higher heating rate, the network is further from its equilibrium state, and the strain increment is delayed, which produces a higher activation temperature.

The thermal strain responses for the epoxy samples are predicted by the model and presented in Fig. 4 as dashed lines. It shows that the model can closely capture the thermal responses of vitrimers.

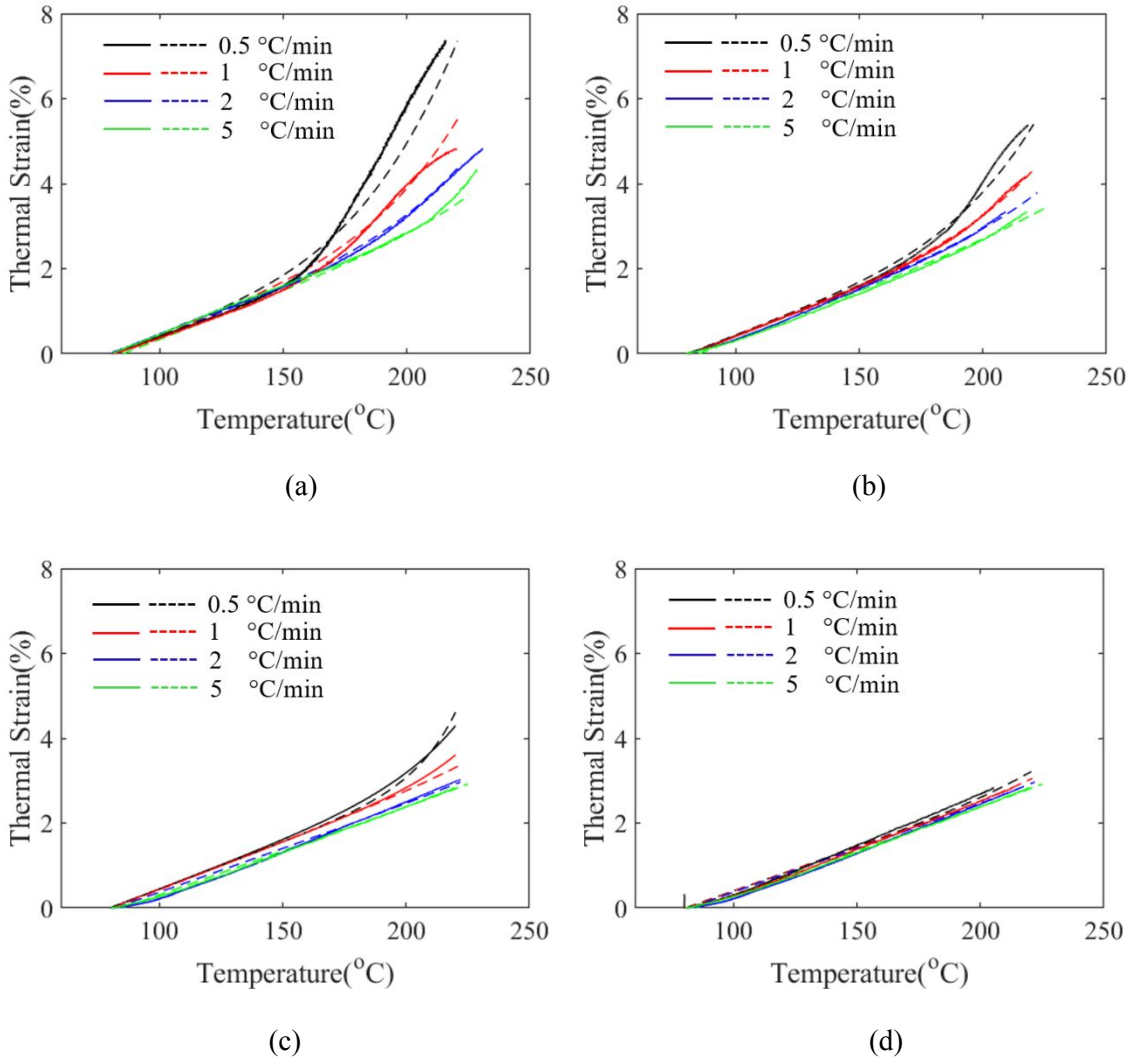

Fig. 4 *Evolution of thermal strain with continuous heating heating profile. The heating rate is 0.5, 1, 2, and 5 °C/min, respectively. The epoxy samples have different catalyst content: (a) 10%, (b) 5%, (c) 1%, and (d) 0 %, respectively. Solid lines: experimental results. Dashed lines: predictions.*

Experimental results in Fig. 4 show that the T_{vi} measured from the thermal expansion tests depends on the catalyst content and the temperature changing rate, which is consistent with the previous experimental observations by Montarnal et al. [18] and Capelot et al. [19, 21]**.** Based on the developed theoretical model, parametric studies were performed to further reveal their influences. Here, we formally define the T_{vi} to be the temperature when

the slope of the thermal strain curve is increased by 5%, as shown in Fig. 5a. Note that T_{vi} can be defined in different ways. For example, it can be defined to be the intersection of the linear regressions for the pre- and post-transition regions. In that case, it will also evolve with heating rate and catalyst content in a similar manner, as shown in Fig. S5 of the Supplementary Materials. To examine the influence of catalyst content, we define the BER activation energy, E_a, changing from 34 to 58 kJ/mol. Higher activation energy suggests a lower catalyst content. The variation in T_{vi} of epoxy vitrimers with different catalyst contents and heating rates is shown in Fig. 5. It is observed that increasing the catalyst content or decreasing the heating rate can both reduce the T_{vi}. However, the T_{vi} value doesn't keep decreasing with the heating rate. Depending on the catalyst content, it tends to saturate when the heating rate is below a critical value. This is because the network is in the quasi-equilibrium state when the temperature changing rate is lower than the structural relaxation rate. As shown in Fig. S3c, within the temperature range of 160-220°C, the structural relaxation time of vitrimer sample with 10% catalyst is ~4000 s – ~850s. The corresponding structural relaxation rate $1/\tau_0$ is ~0.015 min^{-1} – ~0.07^{-1} min. Therefore, T_{vi} is observed to saturate on the order of minutes. The time-dependency of strain evolution is negligible, and thus the T_{vi} only depends on the catalyst content within the network.

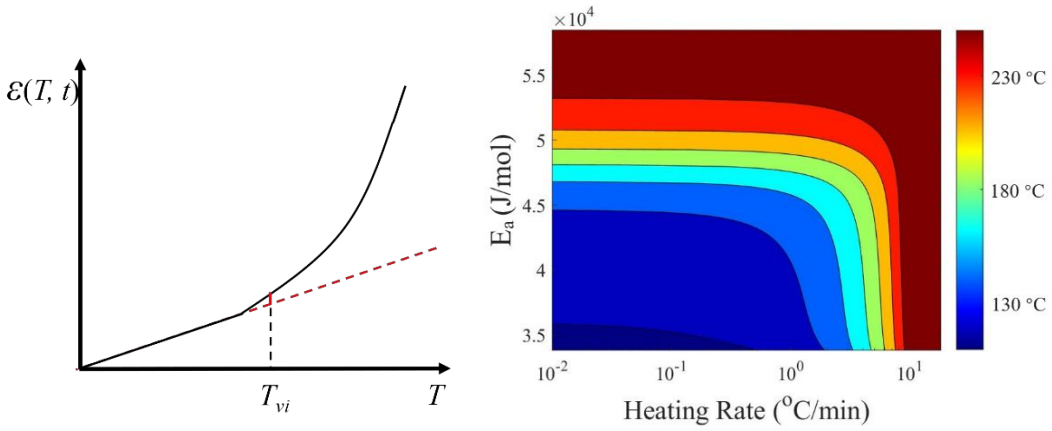

(a) (b)

Fig. 5 *(a) A schematic view showing the definition of BER activation temperature. (b) The BER activation temperature with different BER activation energy and heating rate.*

4.2 Stress relaxation behavior coupled with structural relaxation

4.2.1 Stress relaxation in tension

The stress relaxation behavior of the epoxy vitrimer sample with 10% catalyst was tested in the tension state. During the tests, the temperature was first increased from room temperature to 180 °C at 20 °C/min, and then followed by different stabilization times (0, 3, 6, 8, 11, 15, and 20 min, respectively). After measuring the sample length, a 5% tensile strain was applied and maintained for the rest of the time. The drop of stress was recorded and used to calculate the relaxation modulus.

The relaxation modulus of vitrimer samples and control samples are shown in Fig. S6a of the Supplementary Material. The normalized relaxation modulus is shown below in Fig. 6. It is observed that the normalized relaxation modulus decreases with the extension of stabilization time. Here, we define the characteristic relaxation time to be the time point when the normalized relaxation modulus drops to $1/e$ (e is the natural constant). It is observed to increase from ~3 min to 31 min when the stabilization time increases from 0 to 20 min. The different relaxation rates are due to the varying degrees of structural relaxation during the isothermal stabilization. When the stress relaxation is in a tension state, both structural relaxation and BERs release the internal stress of vitrimers. With a higher stabilization time before the stress relaxation, the epoxy network evolves more towards its equilibrium state, which leads to less thermal strain to be generated during the relaxation and, thus, a lower relaxation rate. It is also observed that the relaxation rate with

a 15 min stabilization almost coincides with that of 20 min stabilization, which suggests that 15 min is the time scale for the epoxy sample with 10% catalyst to reach the equilibrium state at 180 °C. After the stabilization, the relaxation of stress mainly results from BERs. It should be noted that this time scale is consistent with the results of thermal expansion measurements (Fig. 3b), wherein thermal strain evolution tends to be stable after ~15min.

By fitting with the stress-relaxation curves, the parameters in the mechanical components of the theoretical model can be determined. By using six branches, the model can precisely capture the relaxation modulus with different stabilization times. The elastic moduli in these branches are 260, 120, 80, 35, 20, and 5 MPa, respectively. The corresponding relaxation times are 1100, 125, 65, 35, 20, and 5 s, respectively. Note that in previous works [67, 88, 89], only one BER branch was used to capture the stress-relaxation behavior of vitrimers. However, in this study, we intend to investigate more complicated thermomechanical properties of vitrimers, namely the stress-relaxation behaviors (in both tension and compression) coupled with thermal expansion. To improve the model prediction capability, six BER branches are used, which introduces more fitting parameters and are shown below to closely capture the experimental data.

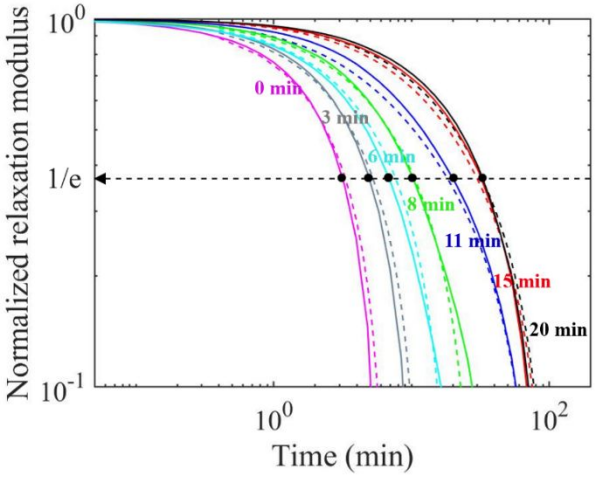

Fig. 6 *Predictions on stretch relaxation behavior for the epoxy with 10% catalyst at different isothermal stabilization time (0,3,6,8,11,15,20 min) at 180 ° C*

The stress relaxation behavior of the epoxy vitrimer sample with different catalyst contents was tested with a 5% tensile strain at different temperatures. All the samples were subject to the same thermal history prior to the stress relaxation. Namely, the temperature first increased from room temperature to the target temperature at 20 °C/min, and then followed by 5min isothermal stabilization times.

Fig. 7 compares the normalized relaxation modulus of these samples. It shows that the relaxation rate increases with temperature and the catalyst content as both two parameters promote the rate of BERs. Even with 1% catalyst, the sample starts to notable release the internal stress with sufficient heating time or high enough temperature. The determined parameters enable the theoretical model to capture the relaxation behaviors. The predictions agree well with the experimental results.

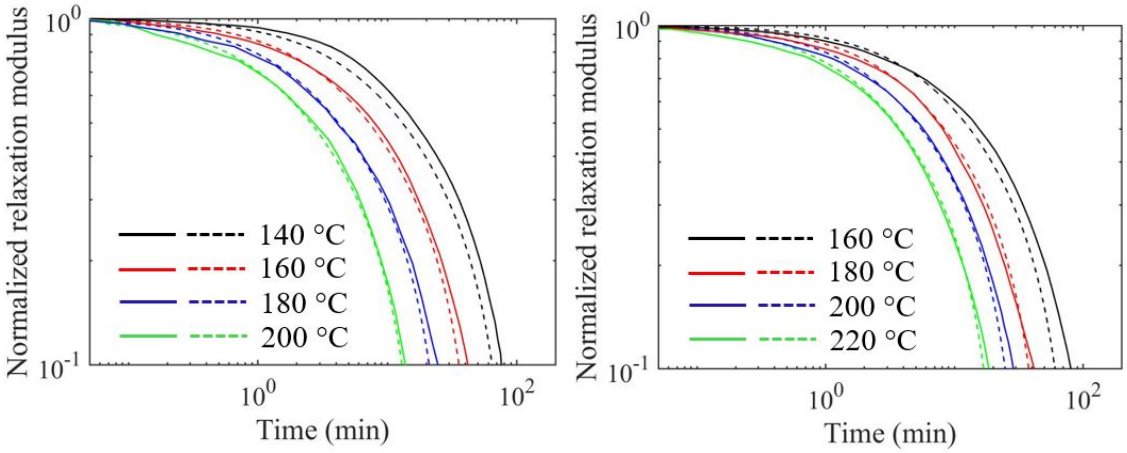

(a) (b)

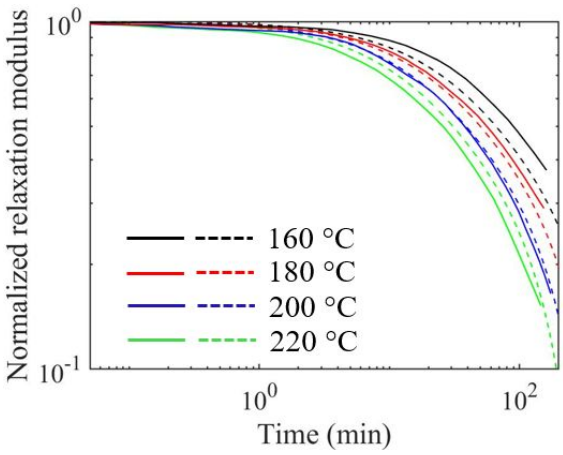

(c)

Fig. 7. *Normalized relaxation modulus of epoxy vitrimer samples in tension with different catalyst contents (a) 10%, (b) 5%, and (c) 1 %. Solid lines: experimental results. Dashed lines: model predictions.*

4.2.2 Stress relaxation in compression

The stress relaxation behavior of the epoxy vitrimer sample with different catalyst contents was evaluated in the compression state, wherein all the samples with the same dimension (5cm × 5cm × 5cm) were heated to the target temperature at 20 ^{o}C/min, stabilized for 5 mins, and compressed with 5% engineering strain. The experimental results are compared in Fig. 8.

Overall, the epoxy vitrimer sample shows unique relaxation behavior when they are being compressed. With a confined boundary condition, structural relaxation tends to increase the sample volume. Therefore, the internal stress first increases until it is surpassed by the amount of BER-induced relaxation. In contrast, the internal stress of the control sample without catalyst keeps increasing until a plateau is reached (Supplementary Material, Fig. S6b). The stress overshot observed in all cases suggests that structural

relaxation is a faster mechanism than the BER-induced stress relaxation. In addition, the peak height and peak position in the relaxation curves are observed to vary with the temperature and catalyst content. With the same catalyst content, higher temperature leads to a higher and earlier peak on the relaxation curves, which results from the faster structural relaxation and higher magnitude of thermal strain. On the other hand, at the same temperature, a higher catalyst content reduces the peak height, and the internal stress tends to relax earlier due to the enhanced BER rates. It is also interesting to observe that for the vitrimer sample with 5% and 10% catalyst, the time corresponding to the peak stress is close to the relaxation time measured in tension state (Fig. 7), namely the time point when the tensile stress of vitrimer sample is dropped to 1/e. This can be telling by comparing the detailed numbers of these two time points in the Supplementary Material (Table S1). However, for the vitrimer sample with 1% catalyst, these two time points are observed to deviate notably, especially when the testing temperature is low. Detailed reason deserves our future study. With the same set of material parameters, Fig. 8 shows that the developed model can accurately predict the relaxation behavior of vitrimer samples in compression.

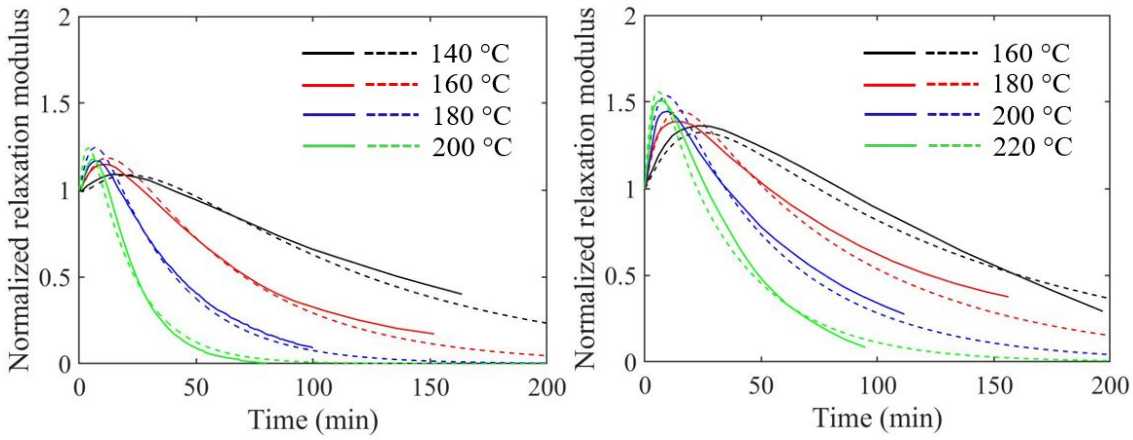

(a) (b)

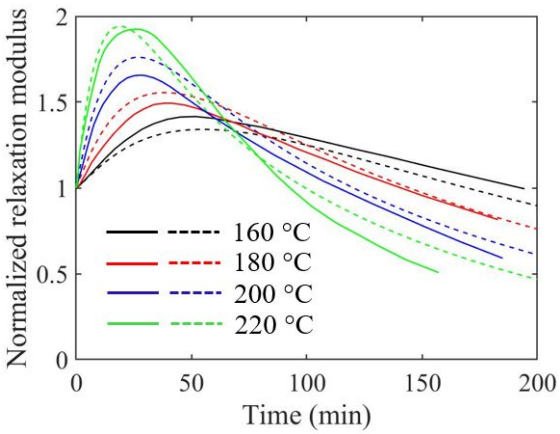

(c)

Fig. 8 *Normalized relaxation modulus of epoxy vitrimer samples in compression with different catalyst contents (a) 10%, (b) 5%, and (c) 1 %. Solid lines: experimental results. Dashed lines: model predictions*

4.3 A BER contribution ratio during the stress relaxation

The BER-induced stress relaxation can be leveraged to repossess thermoset wastes [18, 23, 52], program autonomous shape-changing [6, 7, 16, 18, 22-27, 57-60, 90], and control microscale surface pattern of polymers [91]. However, studies in this paper show that structural relaxation plays a critical role to interpret relaxation behavior. For example, if the vitrimers are processed with tensile stress, a substantial stress releasing may not suggest active BERs but merely the structural relaxation during the topology transition. On the other hand, if the compressive stress is used, vitrimers could already be effectively processed even without dramatic stress releasing. It is therefore important to reveal the contribution of BERs during the stress relaxation process and identify its dependency on the thermal history, such as the heating rate and holding time, which will provide guidelines to design processing conditions for myriad applications of vitrimers.

Here, we use the stress relaxation in the tension state to reveal the contribution of BERs.

As illustrated in Fig. 9, the drop of stress during the relaxation process can be split into two parts, one from BERs and the other one from the structural relaxation. Based on this, we define the BER contribution ratio at a given time point to be:

$$R(t) = \frac{\Delta\sigma_B(t)}{\Delta\sigma(t)}, \tag{9}$$

where $\Delta\sigma$ is the drop of total stress at an infinitesimal time step at t, $\Delta\sigma_B$ is the portion contributed from BERs. If the portion contributed from structural relaxation is $\Delta\sigma_T$, we have: $\Delta\sigma=\Delta\sigma_B+\Delta\sigma_T$. With the effective theoretical model defined in the previous section, we can readily sperate these two relaxation mechanisms and predict the BER contribution ratio with different material and processing parameters.

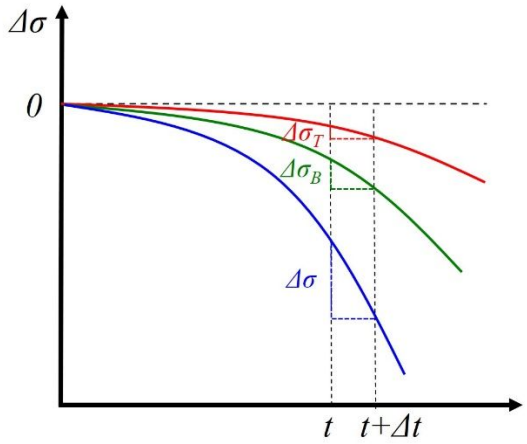

Fig. 9. *A schematic view showing the contribution of BERs on the overall stress relaxation degree at a given time point.*

4.3.1 The effect of catalyst content on the BER contribution ratio

In Fig. 10, the BER contribution ratio (R) is predicted with different temperature, time for relaxation, and catalyst content. Prior to the stress relaxation, the temperature was increased from room temperature to the target temperature at 20°C/min.

From the figure, it is observed that at a given temperature, the BER contribution ratio is low at the early stage of stress relaxation. Most stress releasing results from the structural relaxation (thermal expansion), which suggests the structural relaxation to be a faster mechanism than BER-induced relaxation. As the relaxation proceeds, the BER contribution increases and surpasses the contributions of structural relaxation (when R>50%) at different times, depending on the temperature.

The increment of the BER contribution ratio over time for relaxation is faster with a higher temperature or catalyst content due to the promoted rate of BERs. For the vitrimer with 10% and 5% catalyst, the BER contribution ratio reaches ~100% after 500mins of relaxation at high relaxation temperatures. In these cases, the network reaches the equilibrium state with complete structural relaxation. Further increasing the catalyst content lowers the energy barrier for BERs and promotes the contribution ratio. For example, when the active energy is 9 kJ/mol, R essentially equal to 1 over the entire map (see Supplementary Material, Fig. S8). Overall, during the stress relaxation in the tension of vitrimers, the initial relaxation is dominated by structural relaxation. Using a higher processing temperature or increasing the catalyst content are effective ways to promote the BER contribution ratio.

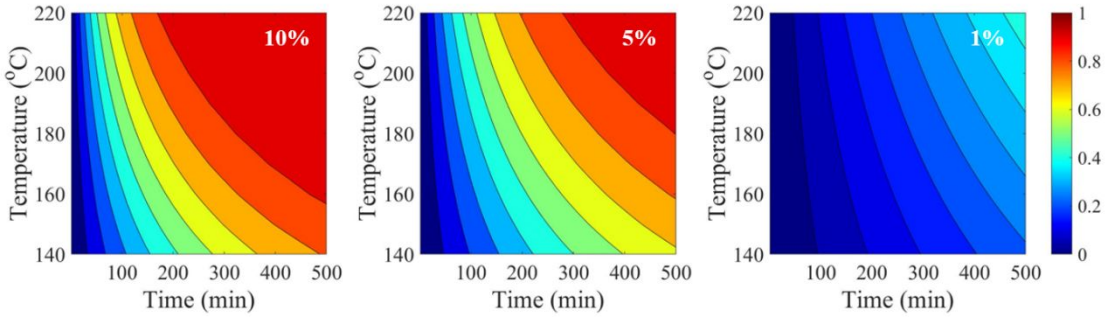

Fig. 10 *The BER relaxation contribution map during the relaxation for epoxy containing (a) 10%,*

(b) 5%, and (c) 1% catalyst as a function of time for relaxation and relaxation temperature.

4.2.2 The effect of holding time and heating rate on the BER contribution ratio

Since the low BER contribution ratio at the early stage of stress relaxation is due to the thermal expansion of the nonequilibrium network, an isothermal holding step prior to the stress relaxation could promote the degree of structural relaxation, and thus increase the BER contribution ratio during the relaxation. Fig.10 shows the predicted BER contribution ratio for vitrimers containing 10% catalyst. Before applying the strain, the temperature was increased from room temperature to the target temperature at 20^{o}C/min and then followed by isothermal stabilization for different times (0-600 min). The BER contribution ratio for vitrimers containing 5% and 1% catalyst are shown in Supplementary Materials (Section S9).

As shown in the figure, increasing the time of isothermal stabilization promotes the BER contribution ratio at all temperatures. During the isothermal stabilization, the vitrimers gradually evolve towards the equilibrium state, which reduces the thermal strain that will be developed during the subsequent stress relaxation, thereby increasing the contribution ratio of BERs. After holding the material at the target temperature for 600 mins, the BER contribution ratio is observed to approach 100% from the very beginning of stress relaxation.

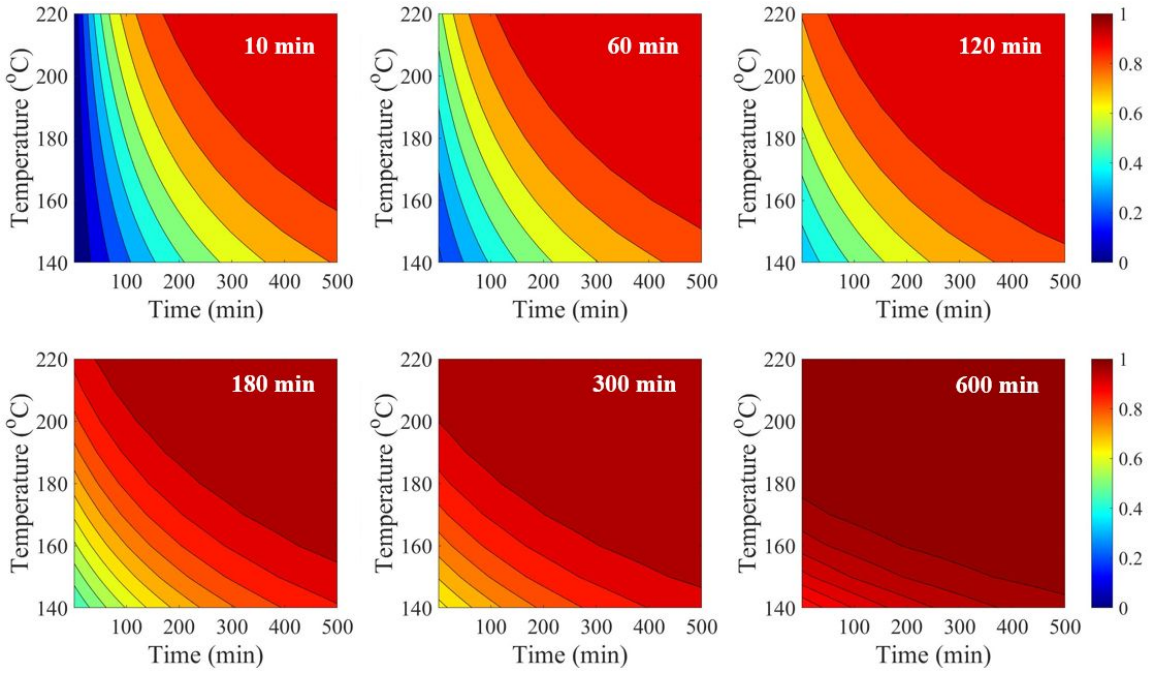

Fig. 11 *The BER contribution ratio during the stress relaxation of epoxy vitrimer containing 10% catalyst. In each figure, the BER contribution ratio is predicted with different isothermal holding times before stress relaxation.*

Another approach to promote the BER contribution ratio is to decrease the heating rate before stress relaxation. Fig.11 shows the BER contribution ratio during the stress relaxation of epoxy vitrimers containing 10% catalyst. Before applying the strain, the temperature was increased from room temperature to the target temperature at different heating rates (0.01, 0.05, 0.1, 0.5, 1, 20 °C/min, respectively). No isothermal holding step was applied before the stress relaxation. The evolution of the BER contribution ratios during the relaxation of epoxy vitrimers containing 5% and 1% catalyst are shown in Supplementary Materials (Section S10). It can be observed that the BER contribution ratio increases with the decrease in the heating rate. Similar to the effect of isothermal holding, a lower heating rate allows more time for the network to evolve to the equilibrium state, which reduces the degree of thermal expansion to be generated during the stress relaxation

and therefore increases the contribution of BER.

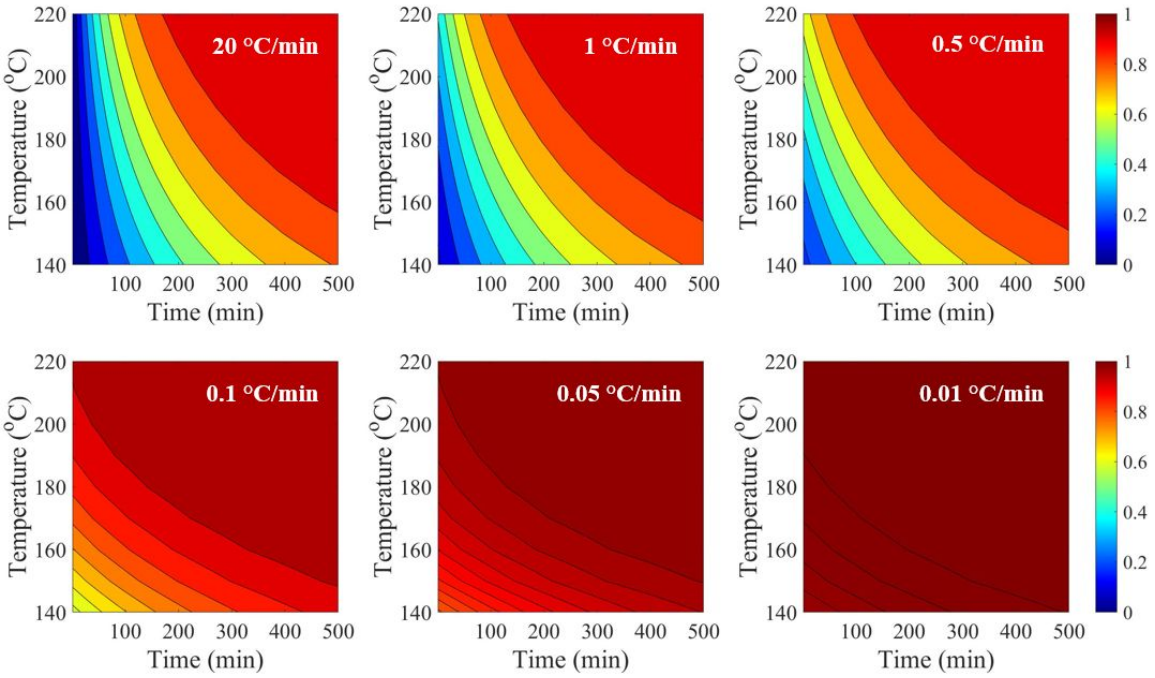

Fig. 12 *The BER contribution ratio during the stress relaxation of epoxy vitrimer containing 10% catalyst. In each figure, the BER contribution ratio is predicted with different heating rates before stress relaxation (0.01, 0.05, 0.1, 0.5, 1, 20 °C/min, respectively).*

5. Conclusion

In this paper, we investigate the rate-dependent response of vitrimer CANs subjected to a change in temperature and mechanical loading during their topology transition. When the temperature is high enough, BERs are activated to rearrange the network topology. However, the microstructure is unable to rearrange instantaneously in response to an external stimulus, and thus the vitrimer CANs are in the nonequilibrium state. Using the thermal expansion tests, the thermal strain evolution is shown to change with the temperature-changing rate. A higher heating rate leads to a slower increment of thermal

strain. Therefore, the BER activation temperature, which is the temperature when the thermal strain dramatically increases, depends not only on the BER catalyst content but also on the heating rate. The effect of structural relaxation on stress relaxation behavior is studied. The evolving thermal strain tends to release the tensile stress while increasing the compressive stress during the stress relaxation. To assist the discussion, a theoretical model was defined based on the concept of fictive temperature. It is able to capture thermal strain evolution during structural relaxation and stress relaxation with confined boundary conditions. Based on the model, the contribution of BERs on the stress relaxation can be readily identified. It shows that structural relaxation is a faster mechanism than the BER-induced stress relaxation, and thus dominates the stress releasing rate at the early stage of relaxation. Using a higher temperature or catalyst content can promote the rate of BERs and hence increase their contribution ratio. Specifically, it shows that an isothermal holding step or a low heating rate before stress relaxation will encourage the network to evolve more towards their equilibrium state, which reduces the thermal strain to be developed during the stress relaxation, thereby increasing the contribution ratio of BERs. Overall, the study in this paper provides valuable insights to understand the thermomechanical properties of vitrimer CANs and can serve as a guideline to design processing conditions for the myriad applications of vitrimer CANs.

Acknowledgements

K.Y. acknowledges support from the National Science Foundation (grant CMMI-1901807).

Appendix A.

Table 1. *Parameters for the theoretical model*

Parameters	Determined values	Description
Parameters for the structural relaxation component		
α	0.027 $^{o}C^{-1}$	Fitting parameters for the BER-induced strain evoluton
β	0.51	
C_1	0.07	Fitting parameters of WLF equation
C_2	18 °C	
α_n	0.00023 $°C^{-1}$	CTE of the epoxy without BER
T_0	80 °C	Reference temperature
τ_{TR_0}	0.15s	Relaxation time
τ_{BR_0}	4.7×10^4s	
Parameters for the mechanical component		
m	6	Number of branches
E_a	44 *kJ/mol,* 47 *kJ/mol,* 55 *kJ/mol*	BER activation energy for vitrimer with 10%, 5%, and 1% catalyst, respectively
E_i	260, 120, 80, 35, 20, 5 *MPa*	Elastic modulus of each branch
τ_i	1100, 125, 65, 35, 20, 5 *s*	Relaxation time of each branch at T_0

References

1. Bower, D.I., *An introduction to polymer physics*. 2002: Cambridge ; New York: Cambridge University Press. xx, 444 p.
2. Aklonis, J.J. and W.J. MacKnight, *Introduction to polymer viscoelasticity. 3rd ed.* 2005: Hoboken, N.J.: Wiley-Interscience. 316 p.
3. Odian, G.G., *Principles of polymerization. 4th ed.* . 2004: Hoboken, N.J.: Wiley-Interscience. xxiv, 812 p.
4. Adzima, B.J., et al., *Rheological and Chemical Analysis of Reverse Gelation in a Covalently Cross-Linked Diels-Alder Polymer Network.* Macromolecules, 2008. **41**(23): p. 9112-9117.
5. Tasdelen, M.A., *Diels–Alder "click" reactions: recent applications in polymer and material science.* Polymer Chemistry.
6. Kloxin, C.J., et al., *Covalent Adaptable Networks (CANS): A Unique Paradigm in Cross-Linked Polymers.* Macromolecules, 2010. **43**(6): p. 2643-2653.
7. Bowman, C.N. and C.J. Kloxin, *Covalent Adaptable Networks: Reversible Bond Structures Incorporated in Polymer Networks.* Angewandte Chemie-International Edition, 2012. **51**(18): p. 4272-4274.
8. Wojtecki, R.J., M.A. Meador, and S.J. Rowan, *Using the dynamic bond to access macroscopically responsive structurally dynamic polymers.* Nature Materials, 2011. **10**(1): p. 14-27.
9. Kolomiets, E. and J.M. Lehn, *Double dynamers: molecular and supramolecular double dynamic polymers.* Chemical Communications, 2005(12): p. 1519-1521.
10. Lehn, J.M., *Dynamers: dynamic molecular and supramolecular polymers.* Progress in Polymer Science, 2005. **30**(8-9): p. 814-831.
11. Lehn, J.M., *Dynamers: Dynamic Molecular and Supramolecular Polymers.* Australian Journal of Chemistry, 2010. **63**(4): p. 611-623.
12. Skene, W.G. and J.M.P. Lehn, *Dynamers: Polyacylhydrazone reversible covalent polymers, component exchange, and constitutional diversity.* Proceedings of the National Academy of Sciences of the United States of America, 2004. **101**(22): p. 8270-8275.
13. Reutenauer, P., et al., *Room Temperature Dynamic Polymers Based on Diels–Alder Chemistry.* Chemistry – A European Journal, 2009. **15**(8): p. 1893-1900.
14. Zou, W.K., et al., *Dynamic Covalent Polymer Networks: from Old Chemistry to Modern Day Innovations.* Advanced Materials, 2017. **29**(14).
15. Jin, Y., et al., *Recent advances in dynamic covalent chemistry.* Chem. Soc. Rev., 2013. **42**(16): p. 6634-54.
16. Scott, T.F., et al., *Photoinduced plasticity in cross-linked polymers.* Science, 2005. **308**(5728): p. 1615-1617.
17. Scott, T.F., R.B. Draughon, and C.N. Bowman, *Actuation in crosslinked polymers via photoinduced stress relaxation.* Advanced Materials, 2006. **18**(16): p. 2128-2132.
18. Montarnal, D., et al., *Silica-Like Malleable Materials from Permanent Organic Networks.* Science, 2011. **334**(6058): p. 965-968.
19. Capelot, M., et al., *Metal-Catalyzed Transesterification for Healing and Assembling of Thermosets.* Journal of the American Chemical Society, 2012.

134(18): p. 7664-7667.
20. Taynton, P., et al., *Heat- or Water-Driven Malleability in a Highly Recyclable Covalent Network Polymer.* Advanced Materials, 2014. **26**(23): p. 3938-3942.
21. Capelot, M., et al., *Catalytic Control of the Vitrimer Glass Transition.* Acs Macro Letters, 2012. **1**(7): p. 789-792.
22. Cromwell, O.R., J. Chung, and Z.B. Guan, *Malleable and Self-Healing Covalent Polymer Networks through Tunable Dynamic Boronic Ester Bonds.* Journal of the American Chemical Society, 2015. **137**(20): p. 6492-6495.
23. Yu, K., et al., *Reprocessing and recycling of thermoset polymers based on bond exchange reaction.* 2014.
24. McBride, M.K., et al., *Photoinduced Plasticity in Cross-Linked Liquid Crystalline Networks.* Adv. Mater. , 2017. **29**: p. 1606509.
25. Mu, X.M., et al., *Photo-induced bending in a light-activated polymer laminated composite.* Soft Matter, 2015. **11**(13): p. 2673-2682.
26. Park, H.Y., et al., *Stress Reduction and Tg Enhancement in Ternary Thiol–Yne–Methacrylate Systems via Addition–Fragmentation Chain Transfer.* 2012.
27. Park, H.Y., et al., *Stress Relaxation by Addition-Fragmentation Chain Transfer in Highly Cross-Linked Thiol-Yne Networks.* Macromolecules, 2010. **43**(24): p. 10188-10190.
28. Chen, X., *A Thermally Re-mendable Cross-Linked Polymeric Material.* Science, 2002. **295**(5560): p. 1698-1702.
29. Ghosh, B. and M.W. Urban, *Induced self-repairing oxetane-substituted chitosan polyurethane networks.* Abstracts of Papers of the American Chemical Society, 2009. **238**.
30. Ghosh, B. and M.W. Urban, *Self-Repairing Oxetane-Substituted Chitosan Polyurethane Networks.* Science, 2009. **323**(5920): p. 1458-1460.
31. Imato, K., et al., *Self-Healing of Chemical Gels Cross-Linked by Diarylbibenzofuranone-Based Trigger-Free Dynamic Covalent Bonds at Room Temperature.* Angewandte Chemie-International Edition, 2012. **51**(5): p. 1138-1142.
32. Lu, Y. and Z. Guan, *Olefin Metathesis for Effective Polymer Healing via Dynamic Exchange of Strong Carbon–Carbon Double Bonds.* Journal of the American Chemical Society, 2012. **134**(34): p. 14226-14231.
33. Chen, Y.L., et al., *Multiphase design of autonomic self-healing thermoplastic elastomers.* Nature Chemistry, 2012. **4**(6): p. 467-472.
34. Cordier, P., et al., *Self-healing and thermoreversible rubber from supramolecular assembly.* Nature, 2008. **451**(7181): p. 977-980.
35. Montarnal, D., et al., *Versatile One-Pot Synthesis of Supramolecular Plastics and Self-Healing Rubbers.* Journal of the American Chemical Society, 2009. **131**(23): p. 7966-+.
36. Phadke, A., et al., *Rapid self-healing hydrogels.* Proceedings of the National Academy of Sciences of the United States of America, 2012. **109**(12): p. 4383-4388.
37. Wang, C., et al., *A Rapid and Efficient Self-Healing Thermo-Reversible Elastomer Crosslinked with Graphene Oxide.* Advanced Materials, 2013. **25**(40): p. 5785-+.
38. Das, A., et al., *Ionic Modification Turns Commercial Rubber into a Self-Healing*

Material. Acs Applied Materials & Interfaces, 2015. **7**(37): p. 20623-20630.
39. Haraguchi, K., K. Uyama, and H. Tanimoto, *Self-healing in Nanocomposite Hydrogels.* Macromolecular Rapid Communications, 2011. **32**(16): p. 1253-1258.
40. Bin Ihsan, A., et al., *Self-Healing Behaviors of Tough Polyampholyte Hydrogels.* Macromolecules, 2016. **49**(11): p. 4245-4252.
41. Mayumi, K., et al., *Fracture of dual crosslink gels with permanent and transient crosslinks.* Extreme Mechanics Letters, 2016. **6**: p. 52-59.
42. Chen, W.-P., et al., *Hydrogel with Ultrafast Self-Healing Property Both in Air and Underwater.* ACS Appl. Mater. Interfaces, 2018. **10**(1): p. 1258-1265.
43. Shi, Q., et al., *Solvent Assisted Pressure-Free Surface Welding and Reprocessing of Malleable Epoxy Polymers.* Macromolecules, 2016. **49**(15): p. 5527-5537.
44. Johnson, L.M., et al., *Controlled degradation of disulfide-based epoxy thermosets for extreme environments.* Polymer, 2015. **64**: p. 84-92.
45. Luzuriaga, A.R.d., et al., *Epoxy resin with exchangeable disulfide crosslinks to obtain reprocessable, repairable and recyclable fiber-reinforced thermoset composites.* Mater. Horiz., 2016. **3**: p. 241-247.
46. Yu, K., et al., *Carbon Fiber Reinforced Thermoset Composite with Near 100% Recyclability.* Advanced Functional Materials, 2016. **26**(33): p. 6098-6106.
47. Taynton, P., et al., *Repairable Woven Carbon Fiber Composites with Full Recyclability Enabled by Malleable Polyimine Networks.* Advanced Materials, 2016. **28**(15): p. 2904-2909.
48. Zhang, Y., A.A. Broekhuis, and F. Picchioni, *Thermally Self-Healing Polymeric Materials: The Next Step to Recycling Thermoset Polymers?* Macromolecules, 2009. **42**(6): p. 1906-1912.
49. Chen, X., et al., *New Thermally Remendable Highly Cross-Linked Polymeric Materials.* Macromolecules. **36**(6): p. 1802-1807.
50. Chen, X.X., et al., *A thermally re-mendable cross-linked polymeric material.* Science, 2002. **295**(5560): p. 1698-1702.
51. Shi, X., et al., *Primary recycling of anhydride-cured engineering epoxy using alcohol solvent.* Polymer Engineering & Science, 2019. **59**(s2): p. E111-E119.
52. Yu, K., et al., *Influence of Stoichiometry on the Glass Transition and Bond Exchange Reactions in Epoxy Thermoset Polymers.* RSC Advances, 2014. **4**: p. 48682-48690.
53. Zhang, B., et al., *Influences of processing conditions on mechanical properties of recycled epoxy-anhydride vitrimers.* Journal of Applied Polymer Science, 2020: p. 49246.
54. Zhang, D., et al., *Influence of cross-linking agent on thermomechanical properties and shape memory effect of styrene shape memory polymer.* Journal of intelligent material systems and structures, 2011. **22**(18): p. 2147-2154.
55. He, X., et al., *Recyclable 3D Printing of Polyimine-Based Covalent Adaptable Network Polymers.* 3D Printing and Additive Manufacturing, 2019. **6**(1): p. 31-39.
56. Shi, Q., et al., *Recyclable 3D printing of vitrimer epoxy.* Materials Horizons, 2017. **4**(4): p. 598-607.
57. Wang, Z., et al., *Reprogrammable, reprocessible and self-healable liquid crystal elastomer with exchangeable disulfide bonds.* ACS Appl. Mater. Interfaces, 2017. **9**: p. 33119-33128.

58. Hanzon, D., et al., *Adaptable Liquid Crystal Elastomers with Transesterification-Based Bond Exchange Reactions.* 2018.
59. Ryu, J., et al., *Photo-origami—Bending and folding polymers with light.* Applied Physics Letters, 2012. **100**(16): p. 161908.
60. Hanzon, D.W., et al., *Adaptable Liquid Crystal Elastomers with Transesterification-Based Bond Exchange Reactions.* Soft Matter, 2018. **14**: p. 951-960.
61. Kyburz, K.A. and K.S. Anseth, *Synthetic mimics of the extracellular matrix: how simple is complex enough?* Annals of biomedical engineering, 2015. **43**(3): p. 489-500.
62. Stowers, R.S., et al., *Matrix stiffness induces a tumorigenic phenotype in mammary epithelium through changes in chromatin accessibility.* Nature biomedical engineering, 2019. **3**(12): p. 1009-1019.
63. Chaudhuri, O., et al., *Hydrogels with tunable stress relaxation regulate stem cell fate and activity.* Nature materials, 2016. **15**(3): p. 326-334.
64. Das, R.K., et al., *Stress-stiffening-mediated stem-cell commitment switch in soft responsive hydrogels.* Nature materials, 2016. **15**(3): p. 318-325.
65. Wang, H. and S.C. Heilshorn, *Adaptable hydrogel networks with reversible linkages for tissue engineering.* Advanced Materials, 2015. **27**(25): p. 3717-3736.
66. McKinnon, D., et al., *Measuring cellular forces using bis-aliphatic hydrazone crosslinked stress-relaxing hydrogels.* Soft Matter, 2014. **10**(46): p. 9230-9236.
67. Yu, K., et al., *Interfacial welding of dynamic covalent network polymers.* Journal of the Mechanics and Physics of Solids, 2016. **94**: p. 1-17.
68. Luo, C., et al., *Chemomechanics in the moisture-induced malleability of polyimine-based covalent adaptable networks.* Macromolecules, 2018. **51**(23): p. 9825-9838.
69. Luo, C., et al., *Effects of bond exchange reactions and relaxation of polymer chains on the thermomechanical behaviors of covalent adaptable network polymers.* Polymer, 2018. **153**: p. 43-51.
70. Luo, C., et al., *Chemomechanics of dual-stage reprocessable thermosets.* Journal of the Mechanics and Physics of Solids, 2019. **126**: p. 168-186.
71. Yu, K., et al., *Dissolution of covalent adaptable network polymers in organic solvent.* Journal of the Mechanics and Physics of Solids, 2017. **109**: p. 78-94.
72. Mao, Y., et al., *A viscoelastic model for hydrothermally activated malleable covalent network polymer and its application in shape memory analysis.* Journal of the Mechanics and Physics of Solids, 2019. **127**: p. 239-265.
73. Shi, X., et al., *A multiscale chemomechanics theory for the solvent–assisted recycling of covalent adaptable network polymers.* Journal of the Mechanics and Physics of Solids, 2020: p. 103918.
74. Yu, K., et al., *Mechanics of self-healing thermoplastic elastomers.* Journal of the Mechanics and Physics of Solids, 2020. **137**: p. 103831.
75. Yu, K., A. Xin, and Q. Wang, *Mechanics of self-healing polymer networks crosslinked by dynamic bonds.* Journal of the Mechanics and Physics of Solids, 2018. **121**: p. 409-431.
76. Vernerey, F.J., *Transient response of nonlinear polymer networks: A kinetic theory.* Journal of the Mechanics and Physics of Solids, 2018. **115**: p. 230-247.

77. J.Vernerey, F., RongLong, and RobertoBrighenti, *A Statistically-Based Continuum Theory for Polymers with Transient Networks.* Journal of the Mechanics and Physics of Solids, 2017. **107**: p. 1-20.
78. Yang, Y., et al., *Detecting topology freezing transition temperature of vitrimers by AIE luminogens.* Nature Communications 2019. **10**: p. 3165.
79. Yu, K., et al., *A Computational Model for Surface Welding in Covalent Adaptable Networks using Finite Element Analysis.* Journal of Applied Mechanics, 2016.
80. Sun, X.H., H.A. Wu, and R. Long, *Thermomechanics of a temperature sensitive covalent adaptable polymer with bond exchange reactions.* Soft Matter, 2016. **12**(43): p. 8847-8860.
81. Kaiser, S., et al., *The Crucial Role of External Force in the Estimation of the Topology Freezing Transition Temperature of Vitrimers by Elongational Creep Measurements.* . Polymer 2020. **204**: p. 122804.
82. Fang, H., et al., *Rheology of the Critical Transition State of an Epoxy Vitrimer.* . Macromolecules 2020. **53**: p. 4855–4862.
83. Tool, A.Q., *Viscosity and the extraordinary heat effects in glass.* J. Am. Ceram. Soc, 1946. **29**(9).
84. Cangialosi, D., et al., *Physical aging in polymers and polymer nanocomposites: recent results and open questions.* Soft Matter, 2013. **9**(36): p. 8619-8630.
85. Ritland, H.N., *Limitations of the Fictive Temperature Concept.* J. Am. Ceram. Soc.,, 1956. **39**(12): p. 403-406.
86. Hensel-Bielowka, S., Z. Wojnarowska, and J.K.M. Paluch, *New insight into relaxation dynamics of an epoxy/hydroxy functionalized polybutadiene from dielectric and mechanical spectroscopy studies.* Colloid and Polymer Science volume, 2014. **292**: p. 1853–1862.
87. Hassan, M.K., et al., *Polymer chain dynamics in epoxy based composites as investigated by broadband dielectric spectroscopy.* Arabian Journal of Chemistry, 2016. **9**(2): p. 305-315.
88. Long, R., H.J. Qia, and M.L. Dunn, *Modeling the mechanics of covalently adaptable polymer networks with temperature-dependent bond exchange reactions.* Soft Matter, 2013. **9**(15): p. 4083-4096.
89. Yu, K., et al., *A Computational Model for Surface Welding in Covalent Adaptable Networks Using Finite-Element Analysis.* Journal of Applied Mechanics-Transactions of the ASME, 2016. **83**(9): p. 091002-091013.
90. Ryu, J., et al., *Photo-origami-Bending and folding polymers with light.* Applied Physics Letters, 2012. **100**(16).
91. Kloxin, C.J., et al., *Mechanophotopatterning on a Photoresponsive Elastomer.* Advanced Materials, 2011. **23**(17): p. 1977-1981.